2024-08-01

Computational Investigation of Layered N_((2-x)) Ni_((2-y)) Co_y TeO_6 (x = 0.0 - 0.5, y = 0.1 - 0.25) For Sodium-Ion Battery Cathodes

Daisy Jennifer Lopez
University of Texas at El Paso

COMPUTATIONAL INVESTIGATION OF LAYERED $Na_{(2-x)}Ni_{(2-y)}Co_yTeO_6$ (x = 0.0 - 0.5, y = 0.1 - 0.25) FOR SODIUM-ION BATTERY CATHODES

DAISY JENNIFER LOPEZ

Master's Program in Physics

APPROVED:

Eunja Kim, Ph.D., Chair

James D. Kubicki, Ph.D.

Mark R. Pederson, Ph.D.

Stephen L. Crites, Jr., Ph.D.
Dean of the Graduate School

COMPUTATIONAL INVESTIGATION OF LAYERED $Na_{(2-x)}Ni_{(2-y)}Co_yTeO_6$ (x = 0.0 - 0.5, y = 0.1 - 0.25) FOR SODIUM-ION BATTERY CATHODES

by

Daisy Jennifer Lopez, B.S.

Thesis

Presented to the Faculty of the Graduate School of

The University of Texas at El Paso

in Partial Fulfillment

of the Requirements

for the Degree of

MASTER OF SCIENCE

Department of Physics

THE UNIVERSITY OF TEXAS AT EL PASO

August 2024

ACKNOWLEDGEMENTS

I am grateful for everyone that I've encountered in my journey. I would first like to thank my advisor, Dr. Eunja Kim, who inspired me and helped me see the beauty in theoretical physics by giving me the opportunity to be a part of her lab, for her never-ending support, guidance, patience, and kindness. I would also like to express my gratitude to my former and current lab mates and friends, Todd Lombardi, Sung-Yup Kim, Nick Wilson, Monica Herrera, and Carlos Hernandez for their continued support and their friendship. I would also like to thank Dr. Harikrishnan Nair and his lab along with Dr. Yohannes Getahun for their parallel experimental work on this project. I would also like to thank my committee members Dr. Mark Pederson and Dr. James Kubicki for their time and consideration in support of my work as well as all the professors in the physics UTEP department who have given me the opportunity to be successful in my pursuit of a higher education. I would also like to thank Elyana Amparan for her kindness and for helping every time I asked for anything.

Outside of the University, I would like to thank my parents, especially my mom, who has always encouraged me to step out of my comfort zone and push myself. My siblings, my best friend, Maria, and all the friends I have made along the way including my coaches and friends at Black Sheep BJJ for making the transition of moving 723 miles away from home easier than expected and helping me build my village. Finally, I would like to express my gratitude for Gabriel for making my life easier and keeping me caffeinated.

ABSTRACT

Sodium-ion batteries have been a source of interest since the 1980's. In 1991, lithium-ion batteries became commercialized and gained popularity, which left studies on sodium-ion batteries behind until recently. The compound $Na_2Ni_2TeO_6$ shows promise and was the principal material studied in this investigation. The goal of this project was to develop sodium-containing novel layered honeycomb oxides for battery cathodes. Density functional theory calculations for three different sodium sites (i.e., Na1, Na2, and Na3) in $Na_2Ni_2TeO_6$ were conducted. Our results indicate that Na atoms in the Na1 site are energetically more favorable than the ones either in Na2 or in Na3 sites. This finding agrees well with the measured XRD data. Chemical tuning was performed to introduce defects to the structure including introducing cobalt and reducing the concentration of sodium. Results indicate AFM cobalt-doped structures are energetically favorable. The sodium-deficient structures show linearity with decreasing sodium concentration.

TABLE OF CONTENTS

LIST OF TABLES

LIST OF FIGURES

CHAPTER 1:

INTRODUCTION

1.1 Sodium-Ion Batteries

When the search for a rechargeable battery began, scientists were making their way down the periodic table looking at alkali metals. Due to being the sixth most abundant element on Earth, sodium has become a primary interest in the search for a new battery. The basic components of a battery are the anode, cathode, and an electrolyte solution. Sodium-ion batteries work similarly to lithium-ion batteries, but the main difference is that in a sodium-ion battery, the sodium ions are the charge carriers. During charging, sodium ions move from the anode to the cathode through an electrolyte solution until a set voltage is reached and during discharging, the sodium ions move from the anode to the cathode through an electrolyte solution. In the current market, batteries contain cathodes generally composed of lithium, cobalt, manganese, and other metallic oxides, however, due to the financial and health-related costs that come with obtaining these elements, along with the rarity and limited resources available, it is crucial to find alternative elements for batteries. Several research studies have been conducted on other alkali metals such as sodium, potassium, rubidium, and caesium as replacements for lithium, but due to the ionic radius of an element playing a crucial role in the diffusion pathways of the cations, sodium has been the most successful in the development for a new battery [12]. Since the first sodium-ion battery material was successfully developed in the early 2000s, there has been an increased interest in sodium-ion battery materials and more research on sodium-based materials being conducted [11].

Figure 1: Chronological timeline of material compositions used for batteries [11].

1.2 Selection of Materials

The main sodium-based structures initially studied were composed of sodium, copper, antimony, tellurium, and oxygen. In 2013, the process of Na extraction and insertion in the interlayers of $Na_2Ni_2TeO_6$ was discovered to be highly reversible, making it an ideal compound for a sodium-ion battery [8]. The $Na_2Ni_2TeO_6$ structure has a $P6_3/mcm$ space group that is due to the Na1, Na2, and Na3 sites [13][14].

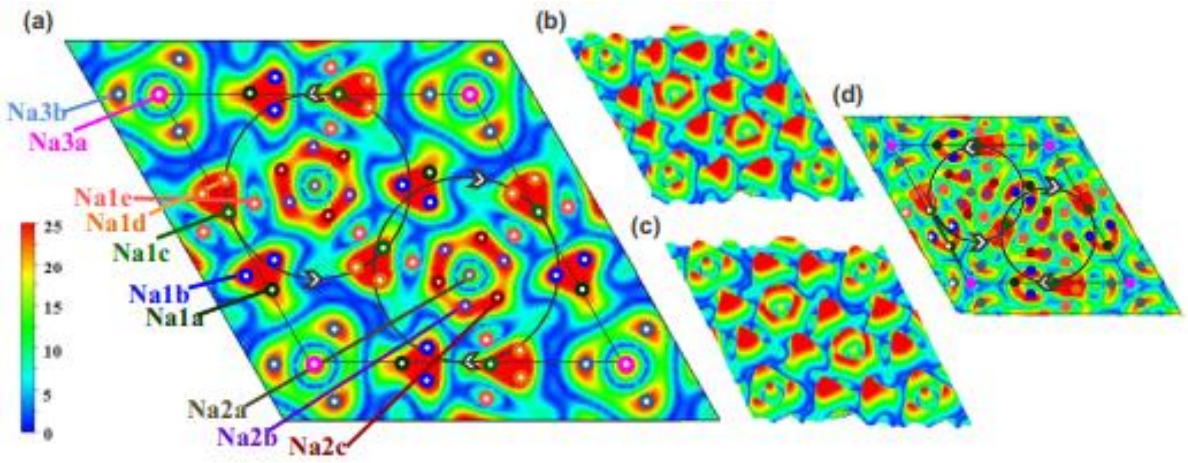

Figure 2: Nuclear density map (a) for $Na_2Ni_2TeO_6$ with labeled Na sites, (b) corresponding 3D maps at layer z = 0.25, (c) z = 0.75, (d) spin direction surrounding Na2 sites [13].

Recent studies on the effect magnetic fields have on lithium-ion batteries indicate that magnetic fields could play a significant role in the charging and discharging cycles of batteries at room temperature by increasing the rate at which the lithium ions flow and diffuse [19]. The $Na_2Ni_2TeO_6$ structure also seems to have AFM ordering when nickel is substituted with cobalt and zinc at low temperatures [3]. However, zinc is not chosen in this study due to a general decrease in sodium-layer thickness when a sodium-based battery material doped with zinc was studied, which could reduce the rate and ease of sodium-ion diffusion compared to a cobalt-doped structure [4]. The addition of cobalt could also result in an increase of length between layers in the c axis that could be crucial to the flow of sodium atoms [5]. With cobalt being a ferromagnetic metal, we decided to dope our supercell structures with AFM cobalt where ISPIN=2.

Molecular dynamics simulations also show that substituting nickel with cobalt, zinc, or magnesium in the $Na_2Ni_2TeO_6$ structure, results in a higher conductivity primarily when nickel is substituted with cobalt [22].

According to studies performed by K. Sau et al., a decrease in sodium concentration by 20% in a sodium-based system is optimal when observing the ionic conductivity of a $Na_2Ni_2TeO_6$ system when the volume is fixed [23]. K. Sau et al. also reported that with an increase in sodium concentration by 20%, Na1 sites tend to be the unfavorable, however, the molecular dynamics simulations showed that sodium ions are accommodated at the Na1 sites at any time during diffusion, while the Na3 sites are the least favorable with sodium ions rarely stopping at the Na3 sites [23]. Magnetic order is also affected when the sodium concentration is increased by 24% [21].

CHAPTER 2:

METHODS

2.1 Density Functional Theory Calculations

The density functional theory (DFT) calculations in this study were carried out using the Vienna Ab-Initio Simulation Package (VASP) at the Texas Advanced Computing Center (TACC) [14][15]. The Perdew-Burke-Ernzerhof (PBE) exchange-correlation functional was also used for all calculations performed in this study [19]. A plane wave basis set with an energy cut-off of 500 eV was used for all calculations [14][15]. A gamma-centered k-point mesh of (7x7x5) was used for unit cell calculations. A k-point mesh of (5x1x3) was used for the (1x5x1) supercells and k-point mesh of (3x3x3) for the (2x2x1) supercells. Convergence testing was conducted to determine the best k-point mesh for the unit cell calculations. Two supercell structures were created by expanding the favorable unit cell with the sodium atoms at the Na1 sites; the first cell was expanded (1x5xl) and a second supercell was expanded (2x2x1). The (1x5x1) supercell was created to directly compare our theoretical work and the Nair group's experimental work. The volume remained constrained for all calculations performed. All figures were modeled using VESTA, the X-ray Diffraction patterns were made using XMGRACE, and the bulk modulus was calculated using EOSFit GUI Birch-Murnaghan Equations of State (EoS) [17][24][6]. All calculations except for the calculations done for the $Na_2Ni_{1.8}Co_{0.2}TeO_6$ structures were not spin polarized calculations.

2.2 Unit Cell with Three Sodium Sites and Interstitial Calculations

There are three sites where sodium atoms can be in the $Na_2Ni_2TeO_6$ structure: Na1, Na2, and Na3 sites. Initial DFT calculations were performed to determine the optimal sodium site. Once that was determined, the favorable structure was expanded (1x5x1) to create a supercell. Five different structures were investigated for this initial study. Figure 3 shows the five structures studied including two unit cells with the sodium atoms at the Na1 sites only (Figure 3a and Figure 3b), one unit cell with the sodium atoms at the Na2 sites only (Figure 3c), one structure with the sodium atoms at the Na1 and Na3 sites (Figure 3d), and one structure with the sodium atoms at the Na2 and Na3 sites (Figure 3e).

Table 1: Unit cell parameters with theoretical and experimental values.

$Na_2Ni_2TeO_6$	Theoretical	Experimental (1)	Experimental (2)
a = b (Å)	5.2016	5.2049	5.2018
c (Å)	11.1723	11.1505	11.1447
α = β	90°	-	-
γ	120°	-	-

Table 1 displays the lattice parameters for the theoretical study, (1) an experimental study conducted by Masese et al. [7], and (2) data from the Nair group. The first experimental lattice parameters on the tables were obtained to compare theoretical to experimental values since we did not initially have a precise value from Dr. Nair's experimental group. The second set of experimental lattice parameters listed are updated values from the Nair group. We see there is only a slight difference between our theoretical lattice parameters and the Nair group's experimental lattice parameters.

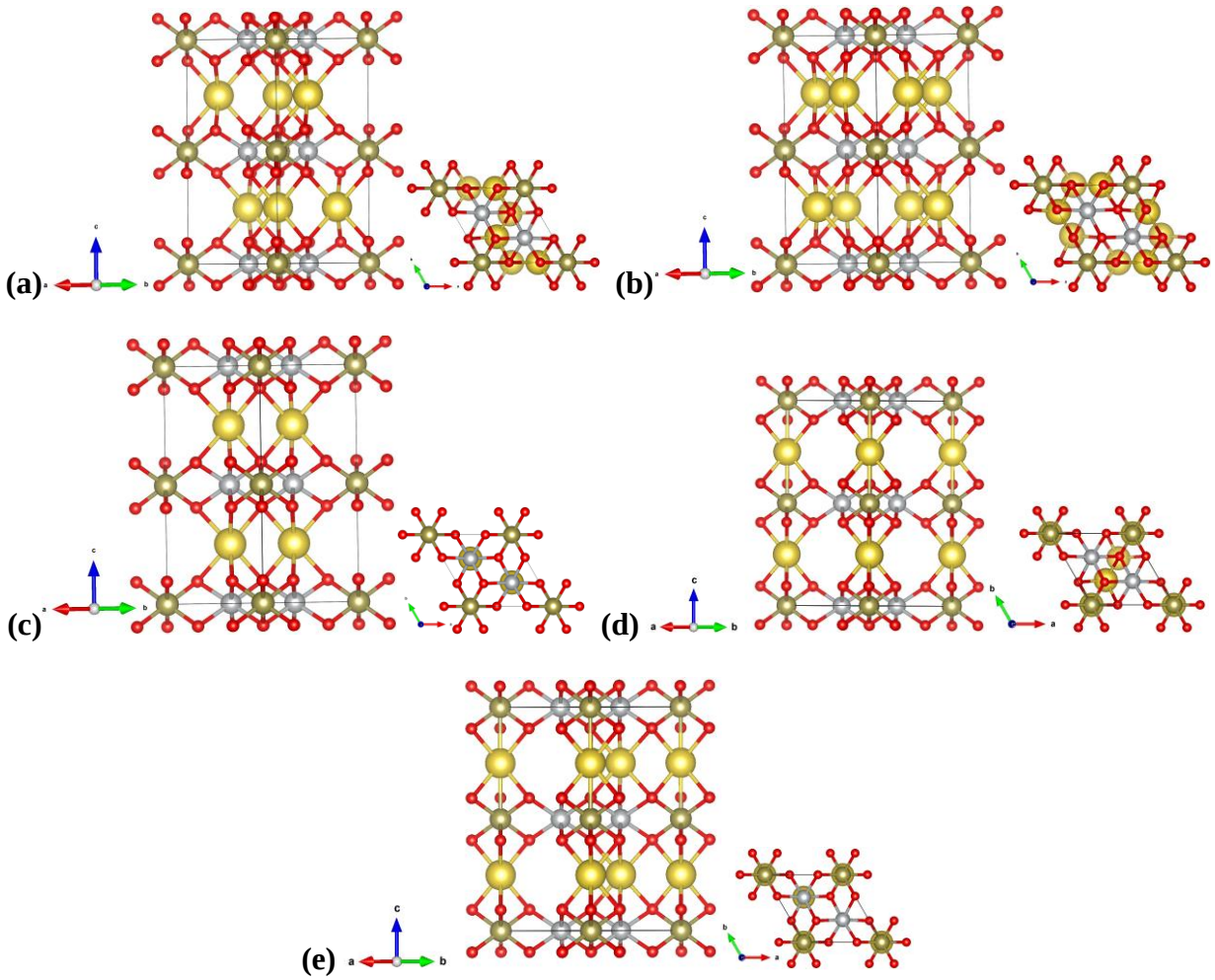

Figure 3: Unit cells (a) Sodium atoms only at Na1 sites, (b) Sodium atoms at different Na1 sites, (c) Sodium atoms at Na2 sites, (d) Sodium atoms at Na1 and Na3 sites, and (e) Sodium atoms at Na2 and Na3 sites. The sodium atoms are yellow, silver atoms are nickel, the bronze atoms are tellurium, and the oxygen atoms are red.

Other calculations included interstitial calculations of sodium with a concentration of 2.5 and 3. Three structures were created for the $Na_{2.5}Ni_2TeO_6$ unit cell displayed in Figure 4 and one structure was created for the $Na_3Ni_2TeO_6$ unit cell displayed in Figure 5. Figure 4a has two sodium atoms on top and three on the bottom. Figure 4b has two sodium atoms on top and three on the bottom as well and Figure 4c has three sodium atoms on top and two on the bottom. Figure 5 has three sodium atoms on top and three on the bottom. All sodium atoms in Figure 5 are at the Na1 sites.

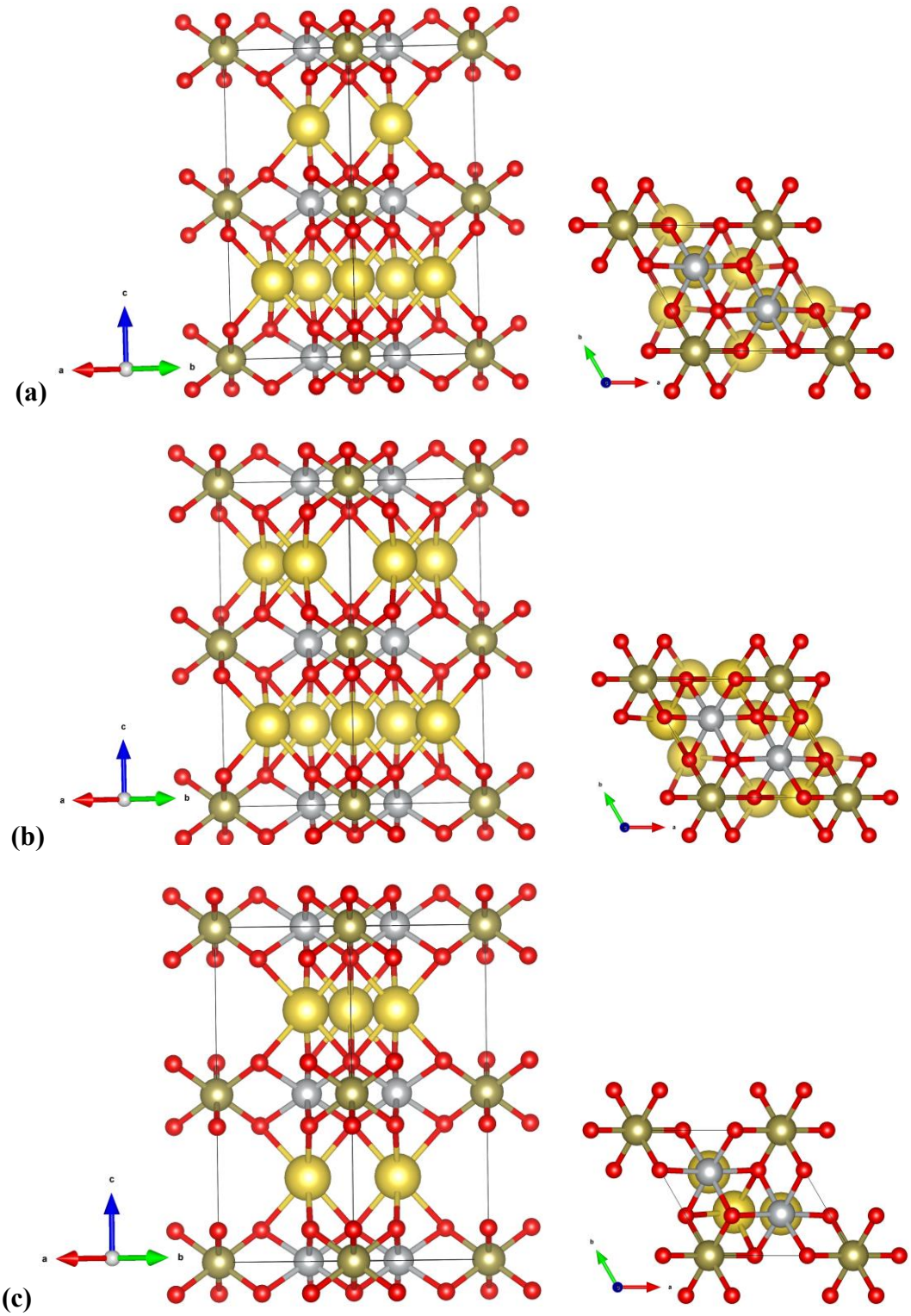

Figure 4: $Na_{2.5}Ni_2TeO_6$ unit cell with sodium atoms at different sites: (a) sodium atoms at Na1 and Na2 sites, (b) sodium atoms only at the Na1 sites, and (c) sodium atoms at the Na1 and Na2 sites. The sodium atoms are yellow, silver atoms are nickel, the bronze atoms are tellurium, and the oxygen atoms are red.

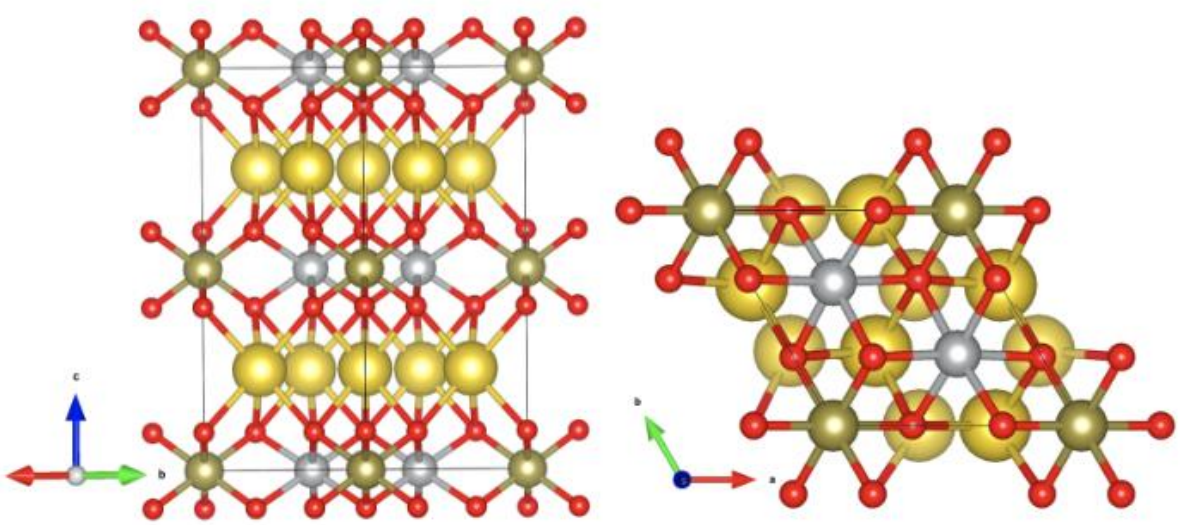

Figure 5: $Na_3Ni_2TeO_6$ unit cell with sodium atoms at the Na1 sites. The sodium atoms are yellow, silver atoms are nickel, the bronze atoms are tellurium, and the oxygen atoms are red.

2.3 Cobalt Doping

One of the goals in this study was to understand if substituting nickel with cobalt in different concentrations would significantly impact the energetics of the material. Four different concentrations of cobalt were used in this study including 0.1, 0.125, 0.2, and 0.25. The (1x5x1) structure was used for the 0.1 and 0.2 cobalt concentrations and the (2x2x1) structure was used for the 0.125 and 0.25 cobalt concentrations. Nearest neighbor calculations were performed on both (1x5x1) and (2x2x1) cobalt doped supercells with the 0.2 and 0.25 concentrations. Figure 6 contains the (1x5x1) supercell structures doped with two cobalt atoms and Figure 7 displays the (1x5x1) supercell with the cobalt atoms placed in different layers. Figure 8 shows the (2x2x1) supercell structure containing two cobalt atoms.

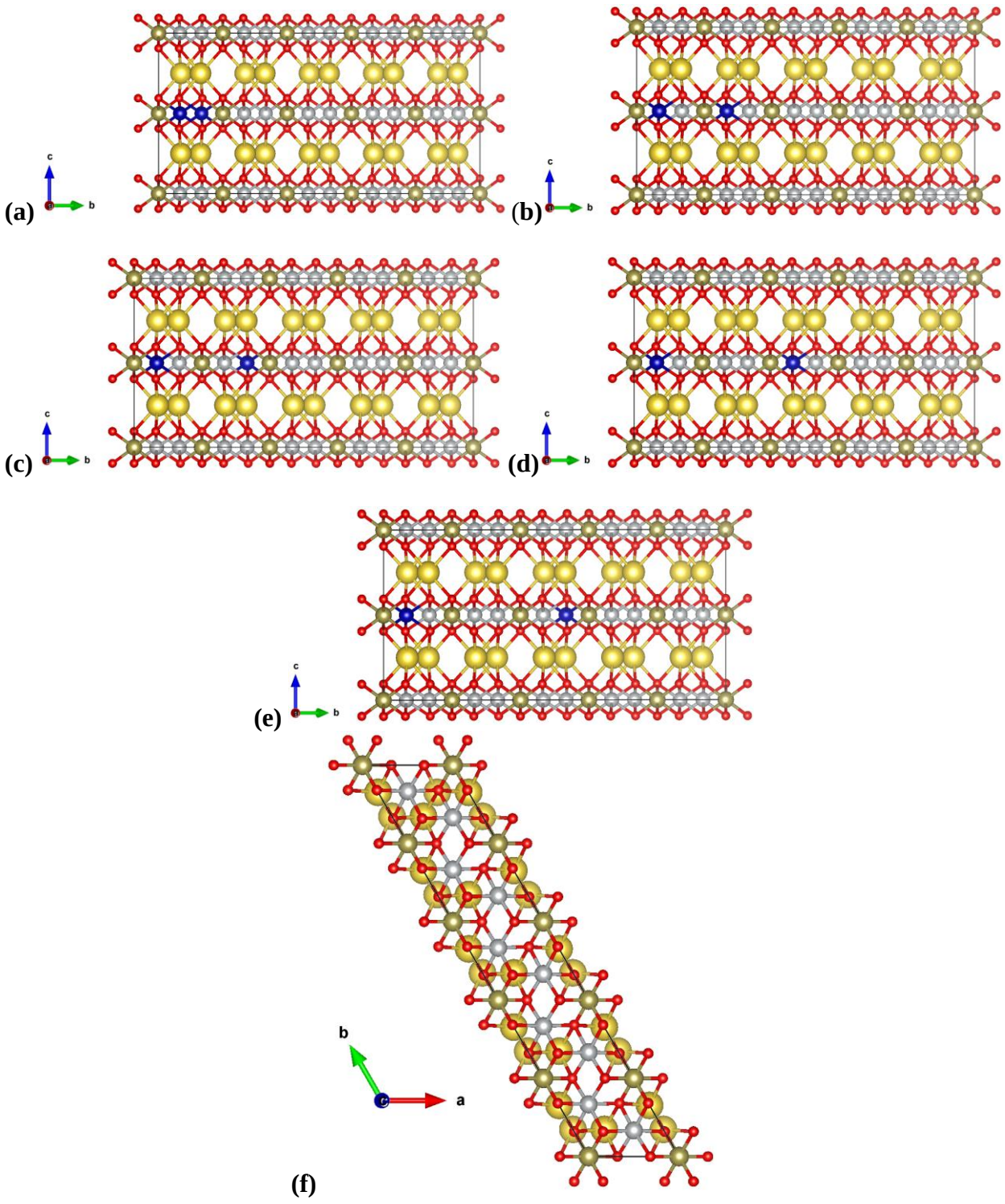

Figure 6: (1x5x1) supercells with cobalt nearest neighbors (a) first nearest neighbor, (b) second nearest neighbor, (c) third nearest neighbor, (d) fourth nearest neighbor, (e) fifth nearest neighbor (f) (1x5x1) supercell from a c-axis point of view. The sodium atoms are yellow, silver atoms are nickel, the bronze atoms are tellurium, the oxygen atoms are red, and the blue atoms are cobalt.

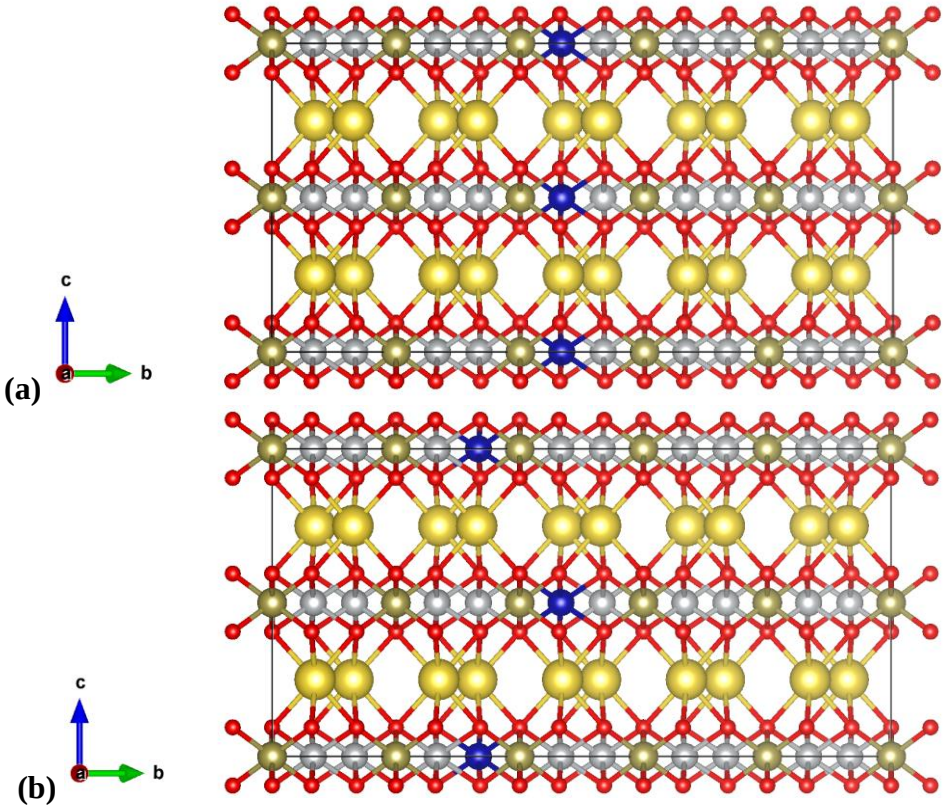

Figure 7: (1x5x1) supercell with cobalt atoms in different layers (a) cobalt is placed directly above, (b) cobalt is placed vertically to the left. The sodium atoms are yellow, silver atoms are nickel, the bronze atoms are tellurium, the oxygen atoms are red, and the blue atoms are cobalt.

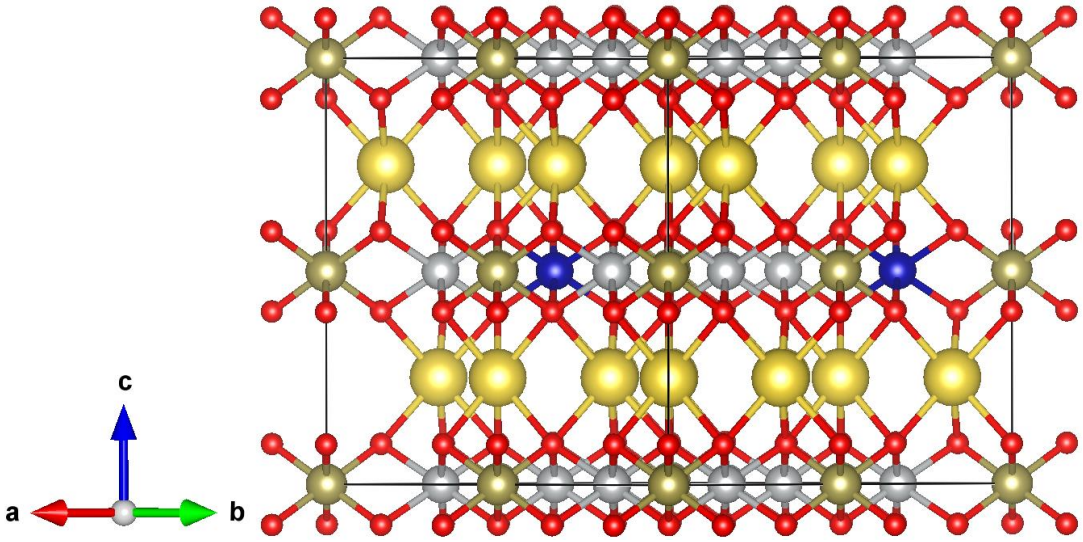

Figure 8: (2x2x1) cobalt-doped $Na_2Ni_{1.8}Co_{0.2}TeO_6$structure. The sodium atoms are yellow, silver atoms are nickel, the bronze atoms are tellurium, the oxygen atoms are red, and the blue atoms are cobalt.

2.4 Sodium Vacancies

The (1x5x1) supercell was created to have a direct comparison between the theoretical and the Nair group's experimental results. A (2x2x1) supercell was created to determine if there was a significant impact on the material's energetics depending on its supercell structure. Sodium vacancies consisted of reducing the concentration of sodium by one atom for each set of calculations. The volume was constrained and was altered to generate energy volume curves for each structure. The concentration of sodium investigated for the (1x5x1) supercell were as follows: Na_2, $Na_{1.9}$, $Na_{1.8}$, $Na_{1.7}$, $Na_{1.6}$, $Na_{1.5}$. Those structures are displayed in Figure 9 (a) and Figure 10 (a). For the (2x2x1) supercell, the concentrations of sodium investigated were $Na_{1.875}$, $Na_{1.75}$, $Na_{1.625}$, and $Na_{1.5}$, and are displayed in Figure 9 (b) and Figure 10 (b).

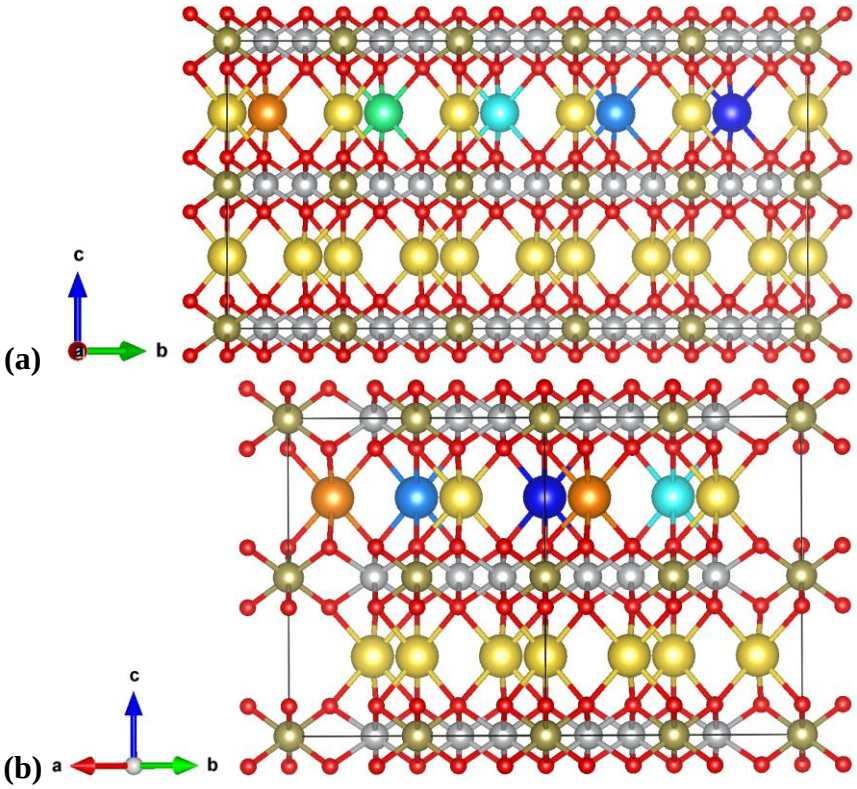

Figure 9: Sodium deficient structures (a) (1x5x1) supercell (b) (2x2x1) supercell. The sodium atoms are yellow, silver atoms are nickel, the bronze atoms are tellurium, the oxygen atoms are red, each different colored atom aside from those noted are the sodium atoms removed to create the vacancies.

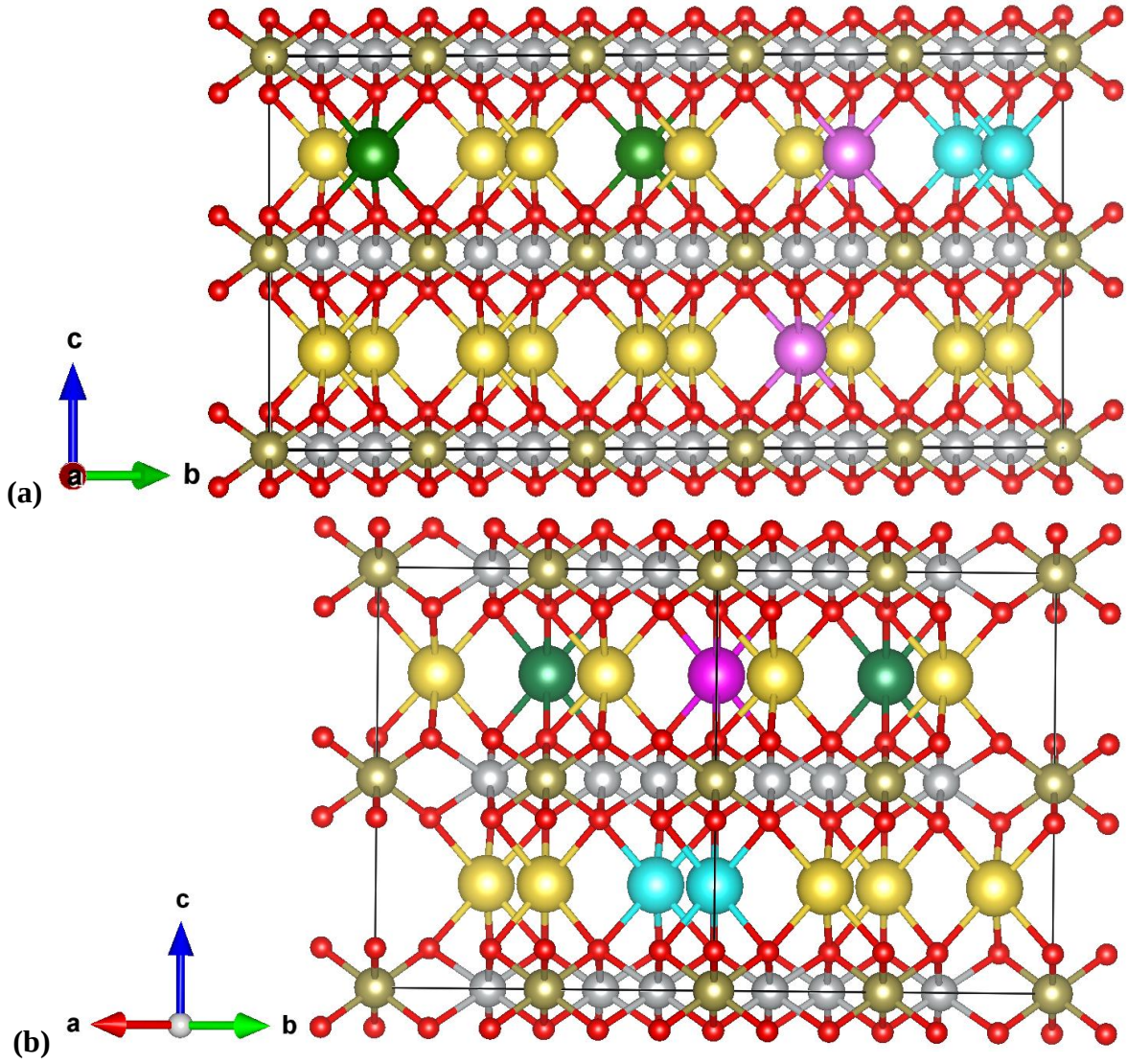

Figure 10: Divacancy structures (a) (1x5x1) supercell (b) (2x2x1) supercell. The sodium atoms are yellow, silver atoms are nickel, the bronze atoms are tellurium, and the oxygen atoms are red. The cerulean atoms represent the sodium atoms removed to create a neighbor divacancy, the green atoms represent the sodium atoms removed to create a horizontal split divacancy, and the pink atoms represent the sodium atoms removed to create a vertical split divacancy.

2.5 Defect Formation Energy Calculations

For the DFT calculations performed, the main source of comparison were the energetics obtained for each calculation. Obtaining structures with the lowest energies were concluded to be the most energetically favorable as those were in their lowest energy states. Because this study included structures that could not have a direct one to one comparison, the defect formation energy was calculated. All structures in this study had energy minimization calculations performed, but the defect formation energies were only obtained for the supercell structures that were cobalt doped and those that had sodium vacancies.

CHAPTER 3:

RESULTS & ANALYSIS

3.1 Parent Compound

The initial structure studied was the $Na_2Ni_2TeO_6$ unit cell with sodium atoms at different sites. There are three positions where sodium atoms can be in the $Na_2Ni_2TeO_6$ structure: the Na1, Na2, and Na3 sites. DFT calculations were carried out on five unit cells with the sodium atoms at different sites and the energetics revealed that the structures with the sodium atoms at the Na1sites were energetically favorable over the structures with the sodium atoms at the Na2, Na1/Na3, and Na2/Na3 sites.

Table 2 contains lattice parameters and energetics for FM structures (a) - (e) where ISPIN = 1. While Table 3 contains lattice parameters and energetics for FM and AFM unit cells at the Na1 and Na2 sites. Figures 11 and 12 are the predicted pressure volume curves for the $Na_2Ni_2TeO_6$ and $Na_{2.5}Ni_2TeO_6$ unit cell structures. Figure 13 is the XRD graph containing the experimental data and the theoretical data for unit cells with the sodium atoms at the Na1, Na2, and Na3 sites.

Table 2: $Na_2Ni_2TeO_6$ energetics and lattice parameters for structures (a) - (e).

$Na_2Ni_2TeO_6$	(a)	(b)	(c)	(d)	(e)
a = b (Å)	5.25362	5.25362	5.25362	5.2016	5.2016
c (Å)	11.28402	11.28402	11.28402	11.1723	11.1723
Volume (Å^3)	269.72	269.72	269.72	261.79	261.79
Total Energy (eV)	-115.86221957	-115.86221953	-115.78798337	-112.15560153	-114.71245428
Bulk Modulus (GPa)	124.95	124.93	116.60	-	-

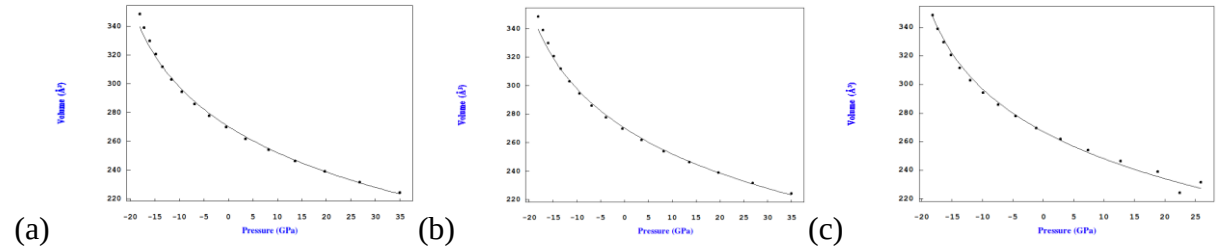

Figure 11: : PV Curve for (a) $Na_2Ni_2TeO_6$structure with sodium atoms at the Na1 sites, (b) $Na_2Ni_2TeO_6$ structure with sodium atoms at different Na1 sites, (c) $Na_2Ni_2TeO_6$ structure with sodium atoms at the Na2 sites

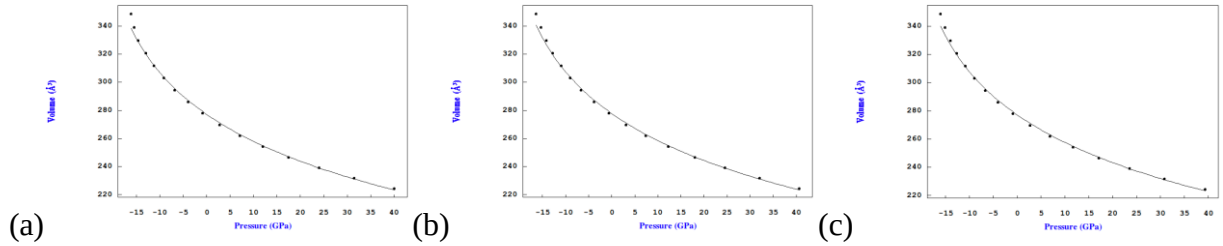

Figure 12: PV Curve for (a) $Na_{2.5}Ni_2TeO_6$ structure with sodium atoms at the Na1 and Na2 sites, (b) $Na_{2.5}Ni_2TeO_6$ structure with sodium atoms at the Na1 sites, (c) $Na_{2.5}Ni_2TeO_6$ structure with sodium atoms at the Na1 and Na3 sites

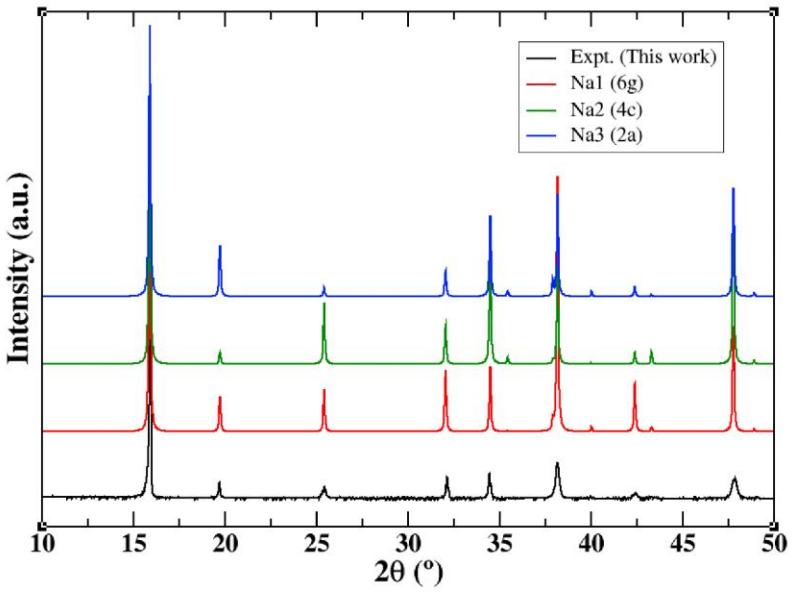

Figure 13: XRD graph comparing experimental XRD data to theoretical XRD pattern for unit cell structure with sodium atoms at Na1, Na2, and Na3 sites.

Table 3: FM and AFM energetics of $Na_2Ni_2TeO_6$.

$Na_2Ni_2TeO_6$	Na1 Site		Na2 Site	
Magnetism	FM	AFM	FM	AFM
Volume (Å³)	269.72	269.72	269.72	269.72
Total Energy (eV)	-115.8622	-118.5214	-115.7880	-118.4979

3.2 Interstitial Structures

After the initial calculations on the structures in Figure 3, the concentration of sodium was increased to obtain the $Na_{2.5}Ni_2TeO_6$ structure. Three structures with a $Na_{2.5}$ stoichiometry were investigated and the DFT calculations for those structures indicated the favorable structure was the structure with the sodium atoms at only the Na1 sites. Because one of our goals was to determine the optimal concentration of sodium, the concentration of sodium was then increased to $Na_3Ni_2TeO_6$. The $Na_3Ni_2TeO_6$ structure had sodium atoms at the Na1 sites only.

Tables 4 and 5 contain the lattice parameters and energetics for $Na_{2.5}Ni_2TeO_6$ and $Na_3Ni_2TeO_6$, respectively. The energetics in the tables show that the structures with the sodium atoms primarily at the Na1 sites are more energetically favorable than those with the sodium atoms at the Na2 sites.

Table 4: Lattice parameters and energetics of $Na_{2.5}Ni_2TeO_6$.

$Na_{2.5}Ni_2TeO_6$	(a)	(b)	(c)
a = b (Å)	5.30563	5.46168	5.46168
c (Å)	11.39575	11.73092	11.73092
Volume (Å³)	277.81	277.81	277.81
Total Energy (eV)	-117.8419	-117.8983	-114.6710
Bulk Modulus (GPa)	120.47	120.67	118.12

Table 5: Lattice parameters and energetics of $Na_3Ni_2TeO_6$.

$Na_3Ni_2TeO_6$	a)
a = b (Å)	5.35765
c (Å)	11.50747
Volume (Å³)	286.06
Total Energy (eV)	-120.0845
Bulk Modulus (GPa)	114.12

3.3 Cobalt Doping

The energetically favorable unit cell was doped with cobalt via substitution. The nickel atoms were substituted for cobalt atoms. The concentration of cobalt differed with supercell structure. The (1x5x1) supercell had a 0.2 concentration of cobalt, while the (2x2x1) supercell had a 0.25 concentration of cobalt. Initial results indicated that the cobalt's position was insignificant, but upon comparing structures with ferromagnetic (FM) cobalt where ISPIN was set to 1 and antiferromagnetic (AFM) cobalt where ISPIN=2, the results indicated that the AFM structures were lower in energy than the FM structures. We note that while the energies differ slightly between FM and AFM structures, there is a correlation between the two structures.

The (1x5x1) and (2x2x1) supercells were also doped with a single cobalt atom, resulting in a concentration of 0.1 for the (1x5x1) supercell and a 0.125 concentration for the (2x2x1) supercell. An X-Ray Diffraction (XRD) pattern was obtained for the $Na_2Ni_{1.9}Co_{0.1}TeO_6$ structure and when compared to an experimental XRD pattern, there was good agreement between the theoretical and experimental structures as shown in Figure 14. The data shown in Figure 15 contains the energetics for the FM $Na_2Ni_{1.8}Co_{0.2}TeO_6$ 1x5x1 structure. The data indicates there is a significant difference between the different structures depending on the cobalt

atoms' positions. The data from Figure 15 is displayed in Table 6 along with the lattice parameters. Figure 16 and Table 7 display the energetics and lattice parameters of the (1x5x1) $Na_2Ni_{1.8}Co_{0.2}TeO_6$ supercell with the cobalt atoms with AFM ordering. This data shows that these structures are lower in energy, leading us to believe that it is more likely that these structures studied have AFM ordering.

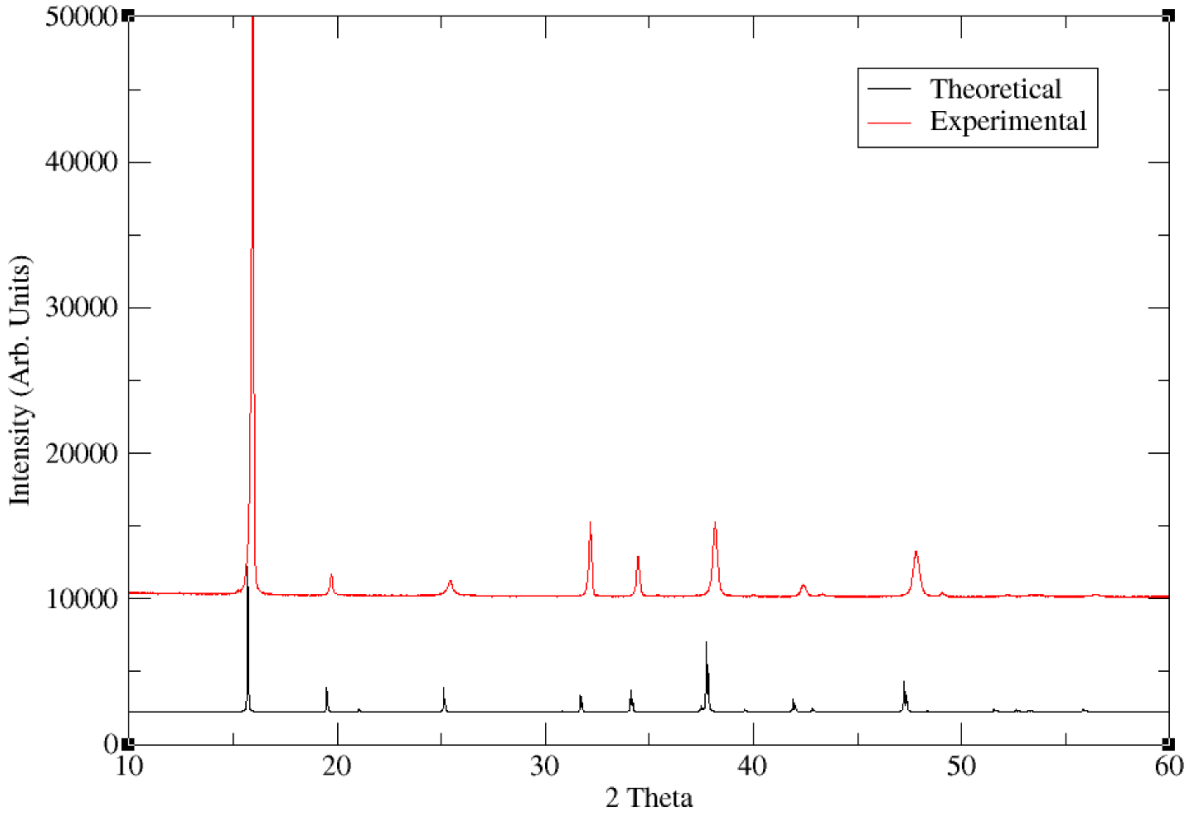

Figure 14: XRD graph for $Na_{2.5}Ni_{1.9}Co_{0.1}TeO_6$ with experimental and theoretical patterns.

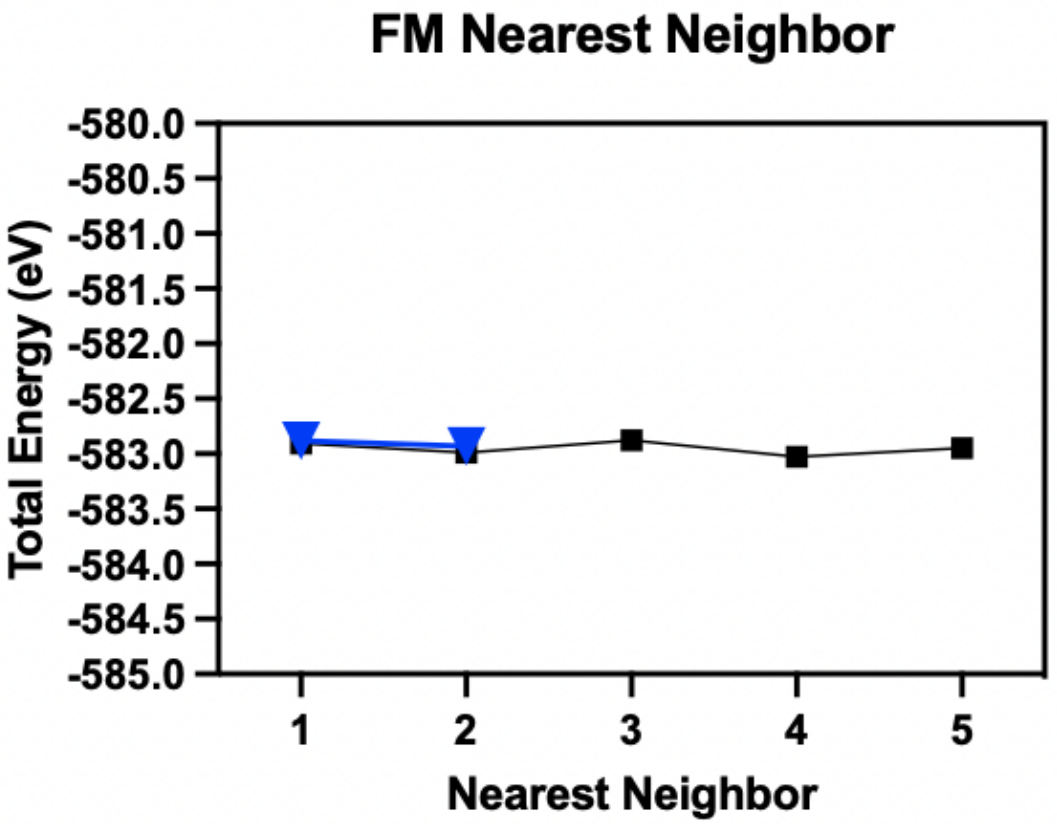

Figure 15: Energetics trend of FM $Na_2Ni_{1.8}Co_{0.2}TeO_6$ (1x5x1) structures.

Table 6: FM lattice parameters and energetics of $Na_2Ni_{1.8}Co_{0.2}TeO_6$ including the structures with cobalt on different layers.

1x5x1	1NN	2NN	3NN	4NN	5NN	Vertical	Split
a (Å)	5.2016	5.2016	5.2016	5.2016	5.2016	5.2016	5.2016
b (Å)	26.008	26.008	26.008	26.008	26.008	26.008	26.008
c (Å)	11.1723	11.1723	11.1723	11.1723	11.1723	11.1723	11.1723
Volume (Å³)	1348.59	1348.59	1348.59	1348.59	1348.59	1348.59	1348.59
Total Energy (eV)	-582.9052	-582.9893	-582.8768	-583.0284	-582.9485	-582.8803	-582.9293

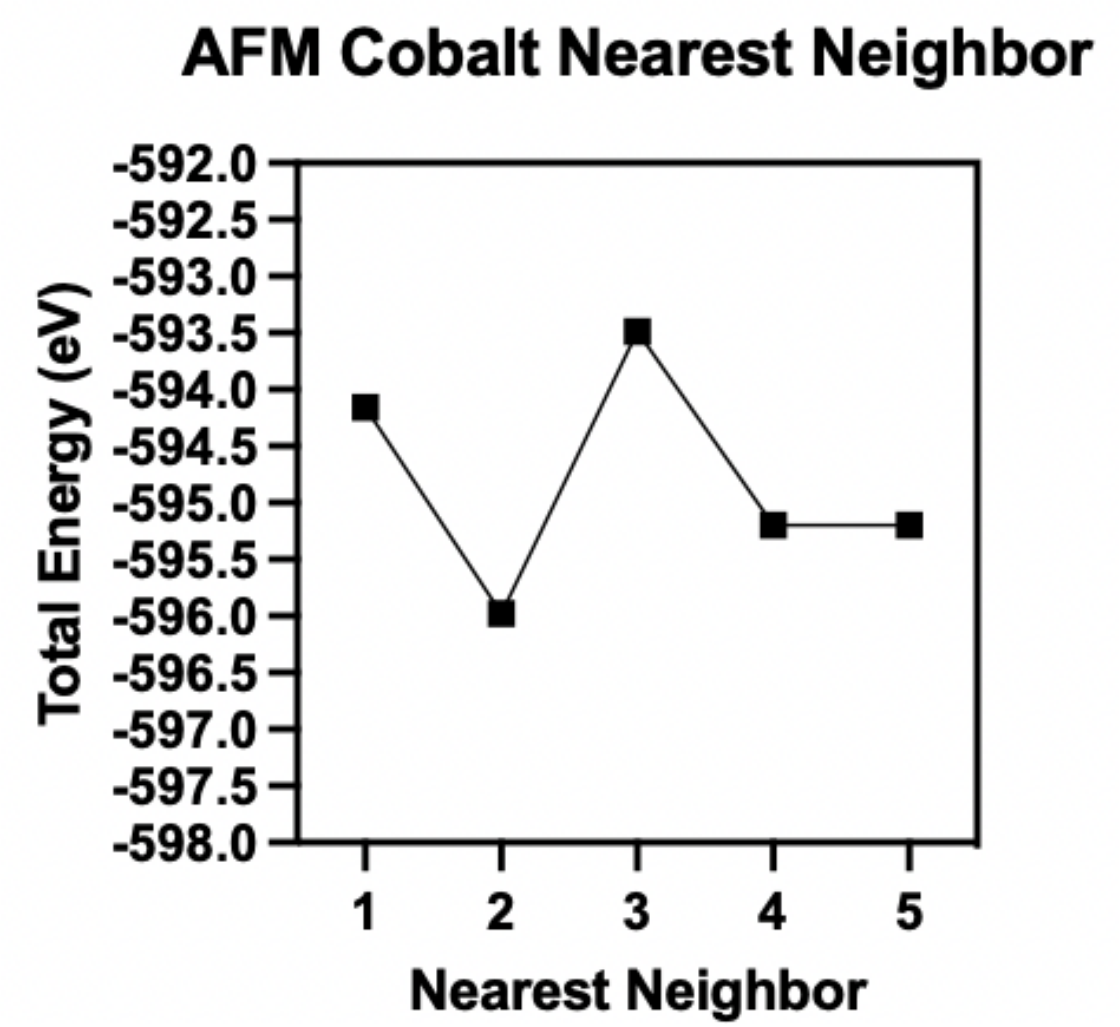

Figure 16: Graph shows energetics trend for AFM cobalt doped (1x5x1) structure.

Table 7: Energetics for $Na_2Ni_{1.8}Co_{0.2}TeO_6$ (1x5x1) structure with AFM cobalt.

1x5x1	1NN	2NN	3NN	4NN	5NN
a (Å)	5.2016	5.2016	5.2016	5.2016	5.2016
b (Å)	26.008	26.008	26.008	26.008	26.008
c (Å)	11.1723	11.1723	11.1723	11.1723	11.1723
Volume (Å³)	1348.59	1348.59	1348.59	1348.59	1348.59
Total Energy (eV)	-594.1562	-595.9769	-593.4879	-595.1997	-595.3165

3.4 Sodium Vacancies

The supercells were also used for sodium vacancy calculations. DFT calculations were performed on the (1x5x1) supercell with sodium concentration ranging from 2.0 to 1.5. The concentration of sodium for the (2x2x1) supercell also ranged from 2.0 to 1.5 with slightly different sodium concentrations due to the difference in total number of atoms between the two supercell structures. Additionally, divacancy calculations were performed on both supercell structures. Three types of divacancy calculations were performed: neighbor divacancy, a vertical split divacancy, and a horizontal split divacancy. Our results indicate that the horizontal split divacancy was energetically more favorable compared to the other two types of divacancies. The defect formation energies are shown in Figure 19.

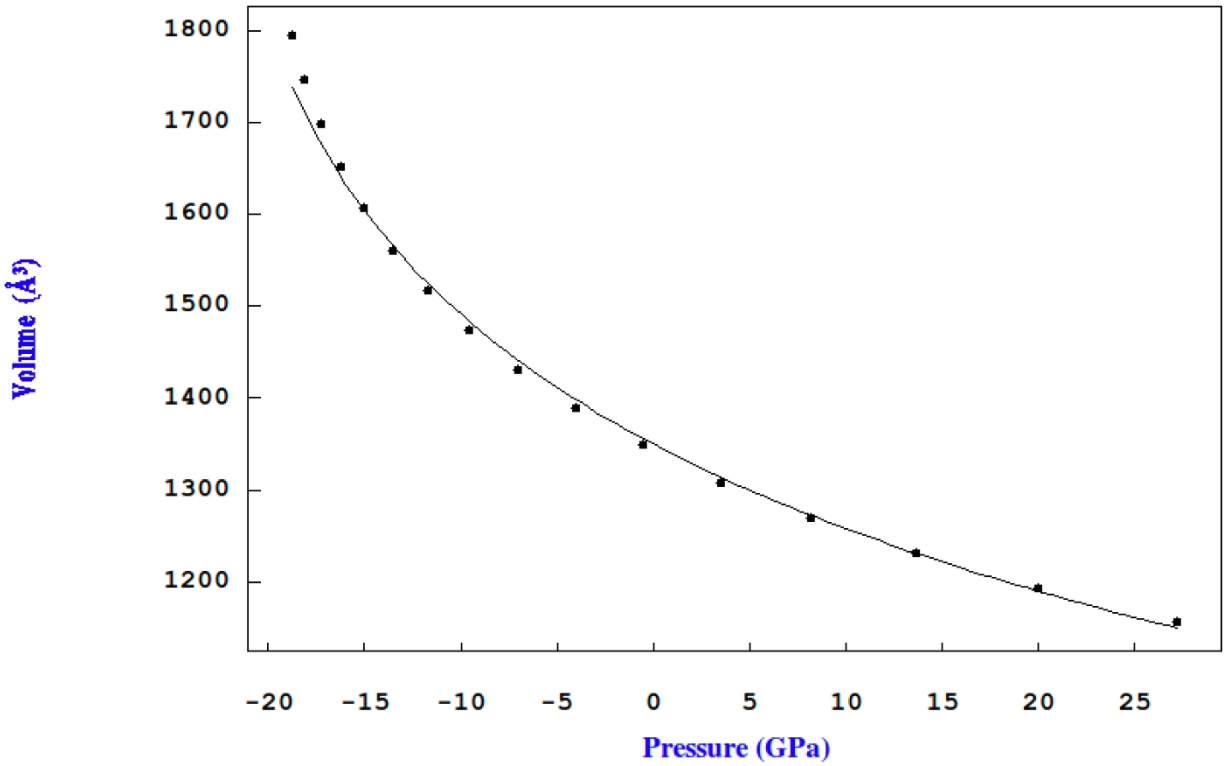

Figure 17: PV Curve for $Na_2Ni_2TeO_6$ (1x5x1) supercell.

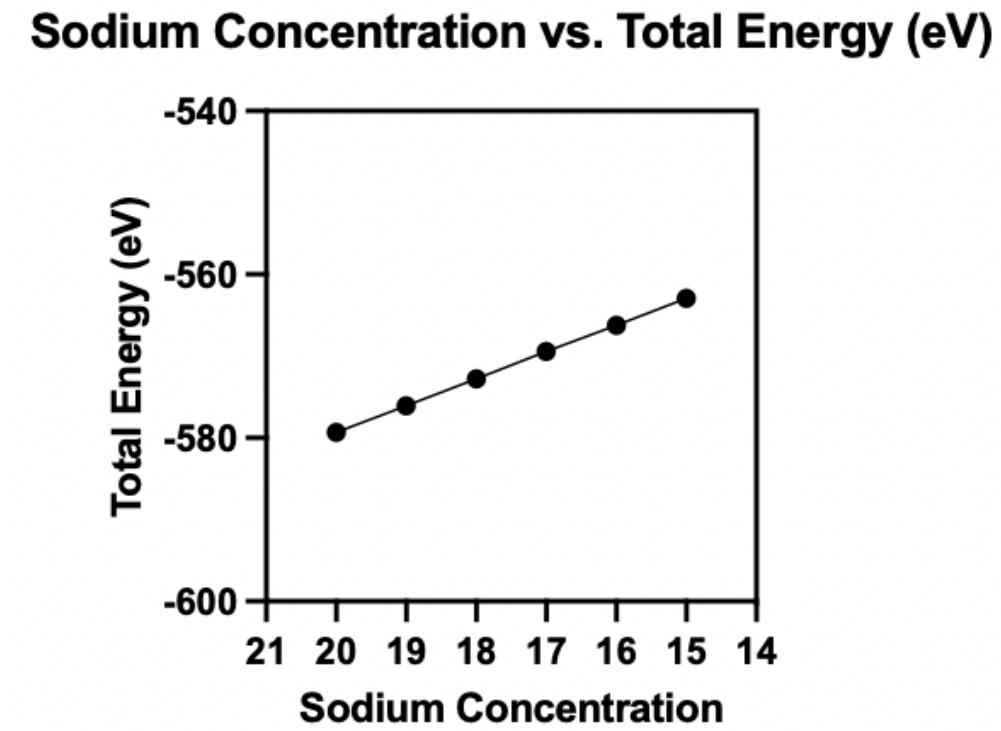

Figure 18: Energetics for $Na_2Ni_2TeO_6$ (1x5x1) structure with sodium vacancies.

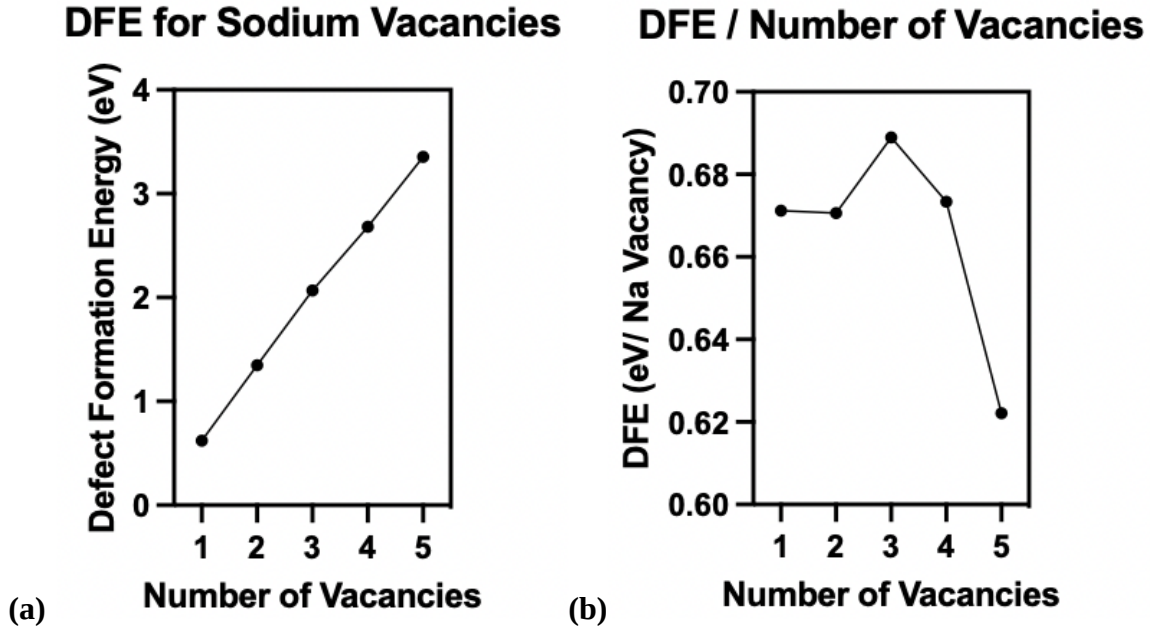

Figure 19: Defect formation energies (a) for (1x5x1) structures with sodium vacancies, (b) for (1x5x1) structures with sodium vacancies divided by the number of vacancies.

CHAPTER 4:

CONCLUSION

4.1 Optimal Structure

From the initial calculations performed on the unit cells with the sodium atoms at Na1, Na2, Na1Na3, and Na2Na3 sites, the energetics suggest that the optimal structure is the one with the sodium atoms at the Na1 sites with an antiferromagnetic moment. The results for the nearest neighbor calculations on the $Na_2Ni_{1.8}Co_{0.2}TeO_6$ (1x5x1) supercell with the AFM cobalt atoms suggest that the position of the cobalt atoms plays a significant role in the energetics of the material. For the $Na_2Ni_{1.9}Co_{0.1}TeO_6$ (1x5x1) supercell, the theoretical XRD pattern agrees with the experimental XRD pattern. For the structures with the sodium vacancies, the results indicate a linear relationship with decreasing sodium concentrations suggesting that this material is ideal for the sodium-ion battery cathode.

4.2 Future Work

The work in this study lays the groundwork for AFM calculations as well as future molecular dynamics simulations to further study diffusion and mechanical properties crucial for the development of sodium-ion battery cathodes for large scale storage. The work presented in this study is only a small view of the potential that sodium-ion materials have for battery applications.

REFERENCES

[1] Aguesse, F., Amo, del, Laida Otaegui, Eider Goikolea, Rojo, T., & Singh, G. (2016). Structural and electrochemical analysis of Zn doped Na3Ni2SbO6 cathode for Na-ion battery. *Journal of Power Sources*, *336*, 186–195.

[2] Bera, A. K., & Yusuf, S. M. (2020). Temperature-Dependent Na-Ion Conduction and Its Pathways in the Crystal Structure of the Layered Battery Material $Na_2Ni_2TeO_6$. *The Journal of Physical Chemistry C*, *124*(8), 4421–4429. https://doi.org/10.1021/acs.jpcc.9b11191

[3] Berthelot, R.; Schmidt, W.; Sleight, A. W.; Subramanian, M. A. Studies on Solid Solutions Based on Layered Honeycomb-Ordered Phases P2-Na2M2TeO6 (M=Co, Ni, Zn). *Journal of Solid State Chemistry* **2012**, *196*, 225–231. https://doi.org/10.1016/j.jssc.2012.06.022.

[4] Darbar, D.; Reddy, M.V.; Bhattacharya, I. Understanding the Effect of Zn Doping on Stability of Cobalt-Free P2-Na0.60Fe0.5Mn0.5O2 Cathode for Sodium Ion Batteries. *Electrochem* 2021, 2, 323–334. https:// doi.org/10.3390/electrochem2020023

[5] Evstigneeva, M. A.; Nalbandyan, V. B.; Petrenko, A. A.; Medvedev, B. S.; Kataev, A. A. A New Family of Fast Sodium Ion Conductors: $Na_2M_2TeO_6$ (M = Ni, Co, Zn, Mg). *Chem. Mater.* **2011**, *23* (5), 1174–1181. https://doi.org/10.1021/cm102629g.

[6] Gonzalez-Platas J, Alvaro M, Nestola F, Angel RJ (2016) EosFit7-GUI: A new GUI tool for equation of state calculations, analyses. and teaching. *Journal of Applied Crystallography*, 49, 1377-1382.

[7] Gupta, A.; Buddie Mullins, C.; Goodenough, J. B. "Na2Ni2TeO6: Evaluation as a Cathode for Sodium Battery". *Journal of Power Sources*, *243*, pp. 817–821. 2013.

[8] Hong, S. Y., Kim, Y., Park, Y., Choi, A., Choi, N.-S., & Lee, K. T. (2013). Charge carriers in rechargeable batteries: Na ions vs. Li ions. *Energy & Environmental Science*, *6*(7), 2067. https://doi.org/10.1039/c3ee40811f

[9] Itoh, Y. (2015). ^{23}Na Nuclear Spin–Lattice Relaxation Studies of $Na_2Ni_2TeO_6$. *Journal of the Physical Society of Japan*, *84*(6), 064714–064714. https://doi.org/10.7566/jpsj.84.064714

[10] Kanyolo, G. M.; Masese, T.; Alshehabi, A.; Huang, Z.-D. Advances in Honeycomb Layered Oxides: Part I -- Syntheses and Characterisations of Pnictogen- and Chalcogen-Based Honeycomb Layered Oxides. arXiv September 11, 2022.

[11] Kanyolo, G. M.; Masese, T. Cationic Vacancies as Defects in Honeycomb Lattices with Modular Symmetries. *Sci Rep* **2022**, *12* (1), 6465. https://doi.org/10.1038/s41598-022-10226-8.

[12] Karna, S. K.; Zhao, Y.; Sankar, R.; Avdeev, M.; Tseng, P. C.; Wang, C. W.; Shu, G. J.; Matan, K.; Guo, G. Y.; Chou, F. C. Sodium Layer Chiral Distribution and Spin Structure of Na 2 Ni 2 TeO 6 with a Ni Honeycomb Lattice. *Phys. Rev. B* **2017**, *95* (10), 104408. https://doi.org/10.1103/PhysRevB.95.104408.

[13] Korshunov, A.; Safiulina, I.; Kurbakov, A. Spin Correlations and Short-Range Magnetic Order in the Honeycomb-Layered $Na_2Ni_2TeO_6$. *Phys. Status Solidi B* **2020**, *257* (3), 1900232. https://doi.org/10.1002/pssb.201900232.

[14] Kresse, G. and Furthmüller, J., "Efficiency of ab-initio total energy calculations for metals and semiconductors using a plane-wave basis set," 1996.

[15] Kresse, G. and Furthmüller, J., "Efficient iterative schemes for *ab initio* total-energy calculations using a plane-wave basis set," *Phys Rev B*, vol. 54, no. 16, p. 1169, Oct. 1996, doi: 10.1103/PhysRevB.54.11169.

[16] Masese, T.; Miyazaki, Y.; Rizell, J.; Kanyolo, G. M.; Takahashi, T.; Ito, M.; Senoh, H.; Saito, T. Unveiling Structural Disorders in Honeycomb Layered Oxide: Na2Ni2TeO6. *Materialia* **2021**, *15*, 101003. https://doi.org/10.1016/j.mtla.2021.101003

[17] Momma, K. and Izumi, F., "VESTA 3 for three-dimensional visualization of crystal, volumetric and morphology data," *urn:issn:0021-8898*, vol. 44, no. 6, pp. 1272– 1276, Oct. 2011, doi: 10.1107/S0021889811038970.

[18] Palomares, V., Serras, P., Villaluenga, I., Hueso, K. B., Carretero-González, J., & Rojo, T. (2012). Na-ion batteries, recent advances and present challenges to become low cost energy storage systems. *Energy & Environmental Science*, 5(3), 5884. https://doi.org/10.1039/c2ee02781j

[19] Perdew, J. P., Burke, K., and Ernzerhof, M., "Generalized Gradient Approximation Made Simple," *Phys Rev Lett*, vol. 77, no. 18, p. 3865, Oct. 1996, doi:10. 1103/PhysRevLett.77.3865.

[20] Ruan, G., Hua, J., Hu, X., & Yu, C. (2022). Study on the influence of magnetic field on the performance of lithium-ion batteries. *Energy Reports*, *8*, 1294–1304. https://doi.org/10.1016/j.egyr.2022.02.095

[21] Samarakoon, A. M., Chen, Q., Zhou, H., & V. Ovidiu Garlea. (2021). Static and dynamic magnetic properties of honeycomb lattice antiferromagnets Na2M2TeO6 , M=Co and Ni. Physical Review. B./Physical Review. B, 104(18). https://doi.org/10.1103/physrevb.104.184415

[22] Sau, K.; Influence of Ion–Ion Correlation on Na+ Transport in Na2Ni2TeO6: Molecular Dynamics Study. *Ionics* **2016**, *22* (12), 2379–2385. https://doi.org/10.1007/s11581-016-1782-2.

[23] Sau, K.; Kumar, P. P. Role of Ion–Ion Correlations on Fast Ion Transport: Molecular Dynamics Simulation of $Na_2Ni_2TeO_6$. *J. Phys. Chem. C* **2015**, *119* (32), 18030–18037. https://doi.org/10.1021/acs.jpcc.5b04087

[24] Turner, P., "XMGRACE." Center for Coastal and Land-Margin Research, Oregon Graduate Institute of Science and Technology, Beaverton, OR, 2005.

CURRICULUM VITA

Daisy Jennifer Lopez earned her bachelor's degree in applied physics from the University of Nevada - Las Vegas in December 2021. Her interest in theoretical physics as well as her boredom while working in the corporate world led her to continue her studies under the guidance of Dr. Eunja Kim at the University of Texas at El Paso where she is currently working towards a master's degree in physics. Daisy has attended several conferences during her time at UTEP where she has presented her research and participated in two research studies. After completing her master's degree, Daisy will be continuing her studies in the physics PhD program at the University of Texas at El Paso continuing her work with her current advisor, Dr. Eunja Kim.

Contact: DAISY.LOPEZ.DJL@GMAIL.COM